PAPER

Check for updates

On-site, rapid and visual method for nanomolar Hg²⁺ detection based on the thymine–Hg²⁺–thymine triggered "double" aggregation of Au nanoparticles enhancing the Tyndall effect†

Xuejiang Chen, Yao Sun, Xiaomei Mo, Qian Gao, Yanan Deng, Miao Hu, Jianmei Zou, Jinfang Nie* and Yun Zhang [ID] *

This work describes a new nanosensor for the simple, rapid, portable, colorimetric analysis of mercury(II) (Hg²⁺) ions by combining the sensitive Tyndall effect (TE) of colloidal Au nanoparticles (AuNPs) with specific thymine–Hg²⁺–thymine (T–Hg²⁺–T) coordination chemistry for the first time. For the TE-inspired assay (TEA), in the presence of Hg²⁺ in a sample, the analyte can selectively mediate the hybridization of three types of flexible single-stranded DNAs (ssDNAs) to form stable rigid double-stranded DNAs (dsDNAs) *via* the T–Hg²⁺–T ligand interaction. Subsequent self-assembly of the dsDNAs with terminal thiol groups on the AuNPs' surfaces led to their "double" aggregation in addition to the lack of sufficient ssDNAs as the stabilizing molecules in a high-salt solution, resulting in a remarkably enhanced TE signal that positively relied on the Hg²⁺ level. The results demonstrated that such a TEA method enabled rapid naked-eye qualitative analysis of 625 nM Hg²⁺ within 10 min with an inexpensive laser pointer pen as an inexpensive handheld light source to generate the TE response. Making use of a smartphone for portable TE readout could further quantitatively detect the Hg²⁺ ions in a linear concentration range from 156 to 2500 nM with a limit of detection as low as 25 nM. Moreover, the developed equipment-free nanosensor was also used to analyze the Hg²⁺ ions in real samples including tap water, drinking water, and pond water, the obtained recoveries were within the range of 93.68 to 108.71%. To the best of our knowledge, this is the first report of using the AuNPs and functional nucleic acids to design a TE-based biosensor for the analysis of highly toxic heavy metal ions.

Introduction

As is known to all, mercury(II) (Hg²⁺) ion is one of the most toxic heavy metal pollutants with the greatest impact on public health. Mercury pollution arises from a variety of natural sources and anthropogenic releases, such as forest fires, volcanic eruptions, burning fossil fuels, gold mining and so on.[1,2] Even when ingested at low concentrations, it can cause damage to the brain, kidneys and lungs of human beings in addition to serious health effects on the nervous, immune, and digestive systems.[3,4] Therefore, highly sensitive and selective Hg²⁺ monitoring is of great importance. To date, there are many techniques available for the detection of Hg²⁺, including atomic absorption spectrometry (AAS),[5,6] atomic emission spectrometry (AES),[7] inductively coupled plasma mass spectroscopy (ICP-

MS),[8] electrochemical methods,[9] high-performance liquid chromatography (HPLC),[10,11] and fluorescence methods.[12,13] Although these instrumental methods can offer high selectivity and sensitivity, they typically require expensive instruments and/or complex procedures, which are cost- and labor-intensive, time-consuming, and non-portable.

To address these issues, alternative efforts have been paid for developing colorimetric approaches which are simple, rapid, and cost-effective, and particularly allow the analytical results to be easily read out with the naked eye. In general, noble metal nanomaterials (primarily gold nanoparticles, AuNPs),[14–16] redox molecules,[17,18] and fluorescent dyes[19,20] are adopted as the colorimetric probes. Among them, using the AuNPs to design colorimetric assays of various analytes of interest including heavy metal ions (*e.g.*, Ag⁺, Pb²⁺, Hg²⁺, Cd²⁺, *etc.*) has attracted over-increasing attention,[21,22] due to their many advantages such as facile synthesis, high surface-to-volume ratio, excellent biocompatibility, and large absorption coefficients.[23,24] Almost all of such sensing systems are based on the analyte-caused aggregation (or anti-aggregation) of the dispersed modified AuNPs, resulting in the solution color change from red to blue

Guangxi Key Laboratory of Electrochemical and Magnetochemical Function Materials, College of Chemistry and Bioengineering, Guilin University of Technology, Guilin 541004, P. R. China. E-mail: zy@glut.edu.cn; Niejinfang@glut.edu.cn; Fax: +86 773 5896839; Tel: +86 773 5896453

(or from blue to red) that is related to their optical property of the localized surface plasmon resonance (LSPR), which can be visually monitored and further quantified by using a UV-vis spectrophotometer.

More recently, another powerful optical property of the colloidal metal nanoparticles like the AuNPs—Tyndall effect (TE)—has been explored for enhanced colorimetric signaling.[25–27] The TE, which is named for the 19th-century British physicist John Tyndall, is defined as the bright "pathway" formed when a light beam passes a colloidal solution due to the scattering effect of the colloidal particles on the light.[28,29] Its intensity positively relies on both of the particle size and concentration.[30] In comparison with the most widely used LSPR method, the TE-inspired assay (TEA) has been demonstrated to offer a significantly improved colorimetric signaling efficiency for detecting a variety of model analytes including inorganic ions (*i.e.*, Ag$^+$ and Hg^{2+}) and small molecules (*i.e.*, cysteamine). However, the previous AuNP-based TEAs still suffer from the disadvantages of multi-step nanoprobe modification, relatively tedious analytical time ($\sim$1 h), and/or more ideal assay specificity remains a big challenge.[25,26]

With these insights, herein we initially describe the proof-of-concept of a new TEA method that combines the unmodified (bare) AuNPs with functional nucleic acids for the rapid, highly specific visual detection and quantification of Hg^{2+} ions at nM levels. Considerable studies have proven that the thymine-rich single-stranded DNA (ssDNA) possesses an excellent selective binding affinity to Hg^{2+}.[31–33] Fig. 1 illustrates the principle of this AuNP-based TEA designed on the basis of the specific thymine–Hg^{2+}–thymine (T–Hg^{2+}–T) coordination chemistry, in which two types of short thiolated ssDNAs (DNA1 and DNA2) and their long complementary ssDNA (DNA3) are used. In the absence of Hg^{2+} in the sample, these sufficiently-flexible ssDNAs with partially-uncoiled bases can make the unmodified AuNPs stably disperse in a solution with high ionic strength after their self-assembly on the nanoparticles' surfaces *via* gold–thiol (Au–S) interactions and/or van der Waals forces, leading to production of a quite weak TE.[34–36] The short ssDNAs (*i.e.*, DNA1 or DNA2 with 12 bases) are specially beneficial to their adsorption on such bare nanoparticle probes.[37] Upon the Hg^{2+}

introduction, the analyte ions can mediate the hybridization of the three types of ssDNAs to form a stable rigid double-stranded DNA (dsDNA) structure by the T–Hg^{2+}–T specific ligand reaction. Subsequently, the aggregation of the AuNPs will take place to generate a significantly-enhanced TE signal, because they are not only brought closer to each other by the terminal thiol groups on both ends of each dsDNA but also lack sufficient flexible ssDNAs as the stabilizing molecules. Residual Hg^{2+} ions would be more likely captured by excessive unfunctionalized DNA3 to exclude their possibility to remove the thiolated oligonucleotides from the particles' surfaces because of their thiophilic nature. The TE response is generated by a red laser pointer pen (635 nm); qualitative or semi-quantitative analysis of the Hg^{2+} level in the sample can be performed just *via* the visual TE change. A smartphone, which has many advantages of portability, lightweight, and on-site imaging and data transmission capability, is additionally used as the TE reader to realize accurate quantitative measurement of the analyte concentration. Both of the laser pointer pen and the smartphone are suitable for use in resource-constrained settings. The main experimental conditions have been optimized, including the AuNP concentration, the DNA concentration, the salt concentration in buffer, and the time and temperature for sample incubation. The results demonstrate that the equipment-free nanosensor developed herein can allow for the simple, sensitive, specific, portable, colorimetric detection of nanomolar Hg^{2+} ions in artificial samples as well as complex real samples like tap water, drinking water and pond water. To the best of our knowledge, this is the first report of using the unmodified AuNPs and functional nucleic acids to design the TEA method for sensing the heavy metal ions like Hg^{2+} within 10 min.

Experimental

Materials and apparatus

Hydrogen tetrachloroaurate(III) (HAuCl$_4$·3H$_2$O) and sodium citrate were the products of Sigma-Aldrich. DNA 1 (5′ TTC CAA CTC GTA-SH 3′), DNA 2 (5′ HS-CGC ATT CAG GAT 3′), DNA 3 (5′ TTC GTG TTG TGT TTC CTG TTT GCG 3′) were purchased from Sangon Biotechnology Co., Ltd. (Shanghai, China). Mercuric chloride (HgCl$_2$) and other metal salts were bought from Xilong Chemical Co., Ltd. (Guangzhou, China). All other chemicals were of analytical grade and used as received without further purification. The used buffer is 10 mM phosphate-buffered saline (pH 7) that contains 450 mM NaCl. Unless stated otherwise, all stock and buffer solutions were prepared with deionized water (with a specific resistivity ≥18.2 MΩ cm) produced from an ultrapure water system (UPS-II-20L) of Chengdu Yuechun Technology Co., Ltd. (Chengdu, China). Hydrophilic polycarbonate nanoporous membranes (Whatman, $\sim$50 nm in average pore size) were obtained from GE Healthcare Life Sciences.

AuNPs were prepared by using a domestic microwave oven. A UV-vis spectrometer (Cary 50, Varian, USA) was used for the optical characterization of dispersed and aggregated AuNPs. The nanoprobes' morphology characterization was conducted
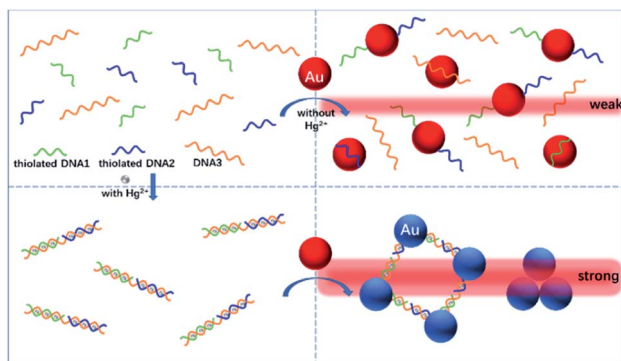

Fig. 1 Schematic representation of the novel TEA method with the bare AuNPs for the colorimetric detection of Hg^{2+} ions based on the specific T–Hg^{2+}–T coordination chemistry.

with a transmission electron microscope (TEM, JEM-2100F, JEOL, Japan). The TE signals were produced with a 635 nm red laser pointer pen (5 mW) that was bought from Deli Group Co., Ltd. (Ningbo, China). Though 445 nm blue or 520 nm green laser pointer pens are also commercially available for the TE production, they might offer relatively higher energy to activate possible optical background interference like fluorescence in real complex samples. Images of all colorimetric and TE results were recorded with a smartphone (Huawei Mate 10).

Synthesis of AuNPs

A microwave-assisted sodium citrate reduction method was adopted to prepare the colloidal AuNPs with ~14 nm in average diameter.[38] In brief, 1 mL of a 1 wt% (w/v) $HAuCl_4 \cdot 3H_2O$ solution and 2 mL of a 1 wt% (w/v) sodium citrate solution were mixed in turn with 97 mL of water. A red-wine-like AuNP solution could be formed after heating this mixture in a home-use microwave oven at high power (800 W) for 8 min. After the resultant AuNP solution was allowed to cool to room temperature (25 °C), it was further diluted with water to the original total volume of 100 mL and finally stored at 4 °C before use. The final particle concentration in such colloidal solution was estimated to be *ca.* 8.8 nM.

Hg^{2+} analysis using the common method with the LSPR signaling

For the LSPR-based method, total 150 μL of 0.5 μM ssDNA probes (50 μL each) was mixed with 50 μL of a Hg^{2+} sample at room temperature (25 °C) for 10 min incubation, followed by addition of 300 μL of a colloidal AuNP solution (4.4 nM). Qualitative or semi-quantitative analysis of Hg^{2+} could be immediately realized through the observation of the color change in reaction solution with the naked eye. The UV-vis spectrum for each reaction mixture was additionally recorded for further quantitative measurement.

Hg^{2+} analysis with the new method with the TE signaling

For the TEA method, the analytical procedures were the same to the above common LSPR approach. After the 10 min reaction for each Hg^{2+} sample, a 635 nm laser pointer pen, which was pre-installed at the bottom of a home-made fully-enclosed device providing stable "black" environmental condition, was utilized to produce the TE signal in the resultant mixture solution to achieve the qualitative or semi-quantitative Hg^{2+} detection. For further quantitative analysis, the corresponding TE image was captured with a smartphone (Fig. S1 in the ESI†). Then, its TE intensity, *i.e.*, the average grayscale (AG) value, was calculated using the grayscale option of the analyze function of the ImageJ processing software. The ΔAG value for each sample was defined as $\Delta AG = AG_{Hg^{2+}} - AG_{blank}$, where $AG_{Hg^{2+}}$ and AG_{blank} were obtained from the Hg^{2+} sample and a blank sample (*i.e.*, buffer without the analyte), respectively. Specificity (selectivity) tests were additionally carried out in the same way but using K^+, Ag^+, Cu^{2+}, Zn^{2+}, Ni^{2+}, Pb^{2+}, Ba^{2+}, Mg^{2+}, Mn^{2+}, Cd^{2+}, Al^{3+}, and Fe^{3+} samples instead of Hg^{2+}.

Results and discussion

First, the feasibility of the Hg^{2+}-triggered aggregation of the AuNPs with enhanced TE *via* the T–Hg^{2+}–T coordination was demonstrated. Fig. 2A shows that the bare 14 nm AuNP solution (4.4 nM) prepared by sodium citrate reduction appears a red color (image a). Their characteristic LSPR band is observed at approximate 520 nm in the UV-vis spectrum (curve a). However, mixing a buffer containing 450 mM NaCl with the AuNP solution led to the color change in the resulting mixture from red to blue (Fig. 2A, image b), which indicates the aggregation of these nanoparticles in such a high-level salt solution. The AuNPs' aggregation was also confirmed by the UV-vis spectrum in which a big decrease was found in the absorbance at 520 nm and a new, broad absorption that stemmed from the aggregated particles concomitantly developed and concentrated at around 690 nm (Fig. 2A, curve b). On the other hand, after the modification of the flexible ssDNAs with partially-uncoiled bases (*i.e.*, the two types of short thiolated DNA 1 and DNA 2 and the long DNA 3) onto these bare AuNPs *via* the Au–S bonds and van der Waals forces, the ssDNA-coated nanoparticles were able to stably disperse in the high-salt-intensity mixture. As a result, the corresponding solution remains red in its color (Fig. 2A, image c) and shows a clear LSPR-related UV-vis absorption peak at ~525 nm with a spectrum profile that is slightly different from that recorded for the bare AuNPs because of the DNA assembly (curves a and c). Moreover, it was interesting to find that incubating these ssDNAs, 10 μM Hg^{2+} and the bare AuNPs in turn resulted in a light blue mixture contained aggregated particles (Fig. 2A, image d), which possessed relatively low and high LSPR absorbance peaks at ~525 and 650 nm, respectively (Fig. 2A, curve d). This may be attributed to the fact that in the presence of Hg^{2+}, the T–Hg^{2+}–T ligand reaction could mediate the
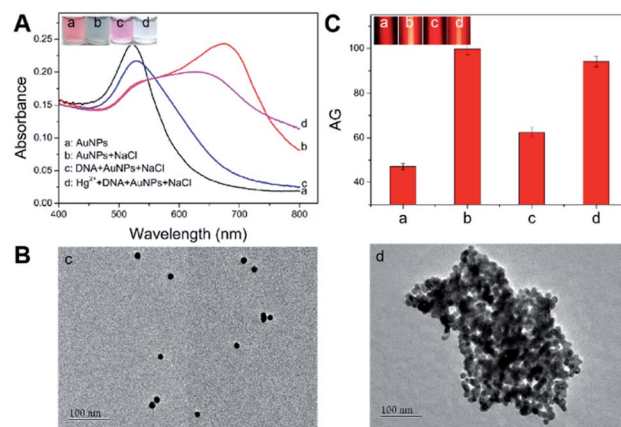

Fig. 2 (A) UV-vis spectra measured from the freshly-prepared AuNPs in the buffer with (a) and without (b) 450 mM NaCl and the bare AuNPs in the buffer containing 450 mM NaCl and three types of ssDNAs in the absence (c) and presence (d) of 10 μM Hg^{2+}. Insets indicate the LSPR-related colorimetric results. (B) Transmission electron microscope (TEM) images obtained from the mixture solutions (c) and (d) shown in (A). (C) TE images (as insets) and their average gray (AG) values measured from the four mixtures shown in (A). Each error bar represents a standard deviation across three replicate experiments.

production of rigid dsDNAs with terminal thiol groups from the hybridization of these ssDNAs to make the AuNPs aggregate through the Au–S binding. In addition, insufficient ssDNAs serving as the stabilizing molecules also promoted the AuNPs' aggregation. The TEM images offer direct experimental evidence of the well AuNPs' dispersion in the absence of the Hg^{2+} (Fig. 2B, image c) and the Hg^{2+}-caused formation of large particle aggregates with hydrodynamic size up to ∼300 nm (Fig. 2B, image d; Fig. S2 in the ESI†). More importantly, both the well-dispersed colloidal unmodified and DNA-stabilized AuNPs displayed clear TE signals (Fig. 2C, images a and c). Such responses could be further remarkably enhanced by the Hg^{2+}-mediated AuNPs' aggregation (Fig. 2C, images b and d), as the light scattering efficiency of the particle probes positively relied on their size.

After demonstrating the feasibility of sensing Hg^{2+} by the new TEA, the bare AuNP concentration was optimized to obtain the highest signal-to-noise ratio. The LSPR and TE signals (with AG values) were recorded from comparatively assaying 10 μM Hg^{2+} samples and blanksamples (buffer without the analyte) using four different AuNP solutions with varying particle concentrations. On can find from Fig. 3A that as the AuNPs' concentration changed (decreased) from 8.8 to 1.1 nM, the LSPR-related red colors of the reaction solutions in the analysis of four blank sample became lighter and lighter and even colorless (top images). The introduction of 10 μM Hg^{2+} led to the aggregation of AuNPs producing four blue mixtures whose color intensity positively depended on the particle levels (Fig. 3A, bottom images). Fig. 3B further shows that the TE responses of the four red reaction mixtures in the cases of blank samples positively relied on the AuNP concentration (top images) and could be dramatically enlarged after the Hg^{2+}-triggered production of aggregated particles with larger scattering efficiency (bottom images). In particular, clear TE signals could still be observed in the completely colorless solution obtained from the analysis of either the blank sample or Hg^{2+} sample with 1.1 nM AuNPs. This comparison study implies that the AuNPs' TE is superior over the most common LSPR in offering a more ideal colorimetric signaling efficiency for visual

analysis of Hg^{2+} ions to achieve the higher detection sensitivity. As additionally provided in Fig. 3C, the AG change (ΔAG) between the Hg^{2+} sample and blank sample (i.e., signal-to-background ratio) peaks at 4.4 nM AuNPs, which is thus recommended as the optimal particle concentration. Moreover, besides the AuNP level, other main experimental conditions had also been optimized for the Hg^{2+} detection, including DNA level, NaCl concentration in the buffer, and reaction time and temperature. The results implied that most of the Hg^{2+}-caused aggregation and TE enhancement of 4.4 nM AuNPs with 0.5 μM functional nucleic acid in the buffer containing 450 mM NaCl could be rapidly completed within 10 min at room temperature (∼25 °C) (Fig. S3–S7 in ESI†).

Next, with the above optimized factors, our new method was adopted to parallelly analyze 10 μM Hg^{2+}, other 12 types of interfering metal ions (100 μM each), and a blank sample to evaluate its analytical specificity, with results shown in Fig. 4. Almost the same LSPR-related red colorimetric results (Fig. 4A), relatively weak TE signals (Fig. 4B) and small AG values (Fig. 4C) were observed from the analysis of the blank sample and 100 μM K^+, Ag^+, Cu^{2+}, Zn^{2+}, Ni^{2+}, Pb^{2+}, Ba^{2+}, Mg^{2+}, Mn^{2+}, Cd^{2+}, Al^{3+}, and Fe^{3+} samples. These results suggested the good dispersion of the AuNPs used in these 13 cases, presumably owing to that no significant interactions took place between these nonspecific ions and the three types of DNAs (which actually acted as the stabilizing molecules after their self-assembly on the nanoprobes' surfaces). In contrast, as expected, the Hg^{2+} assay resulted in the production of a blue reaction mixture showing a quite strong TE response with a large AG value (Fig. 4A–C). In other words, only the analyte ion had triggered the T–Hg^{2+}–T ligand reactions to promote the flexible ssDNAs' hybridization for forming rigid dsDNAs with terminal thiol groups on both ends which in turn made the AuNPs aggregate (closer to each other) via the Au–S binding. The consumed ssDNAs also contributed to the aggregation of the AuNPs under the high-salt condition.

Then, in order to assess the detection performance and advantages of the proposed TEA method, a series of artificial samples in buffer with different Hg^{2+} concentrations ranging from 0 to 6250 nM were analyzed. The results were compared with that obtained from the LSPR strategy. For the traditional method, as presented in Fig. 5A, the Hg^{2+}-caused AuNPs'
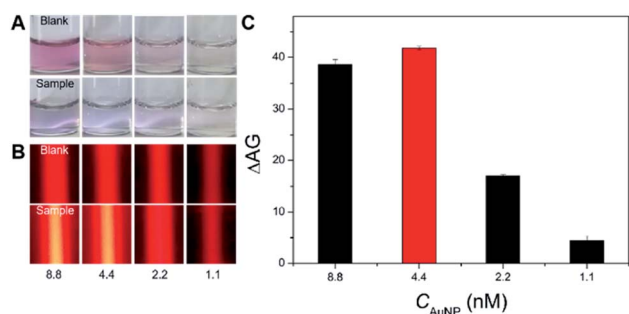

Fig. 3 (A) LSPR-related colorimetric results obtained from the assays of 10 μM Hg^{2+} (bottom) and blank samples (buffer without the analyte; top) using AuNPs of different levels (nM). (B) Corresponding TE signals of the reaction mixtures shown in (A). (C) AG changes (ΔAG) between the Hg^{2+} samples and blank samples shown in (B). Each error bar represents a standard deviation across three replicate experiments.
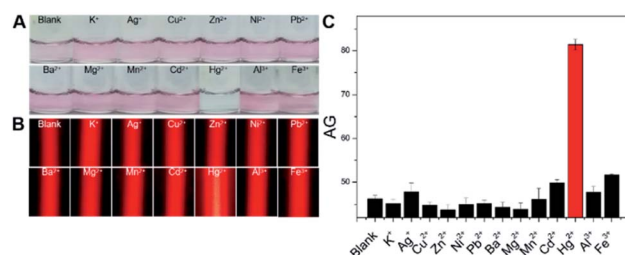

Fig. 4 (A) LSPR-related colorimetric results obtained from the analysis of different samples with 4.4 nM AuNPs: a blank sample (buffer without the analyte), 10 μM Hg^{2+}, and 12 other types of metal ions (100 μM each). (B) TE images of the reaction mixtures shown in (A). (C) The AG values calculated from the TE signals provided in (B). Each error bar represents a standard deviation across three replicate experiments.
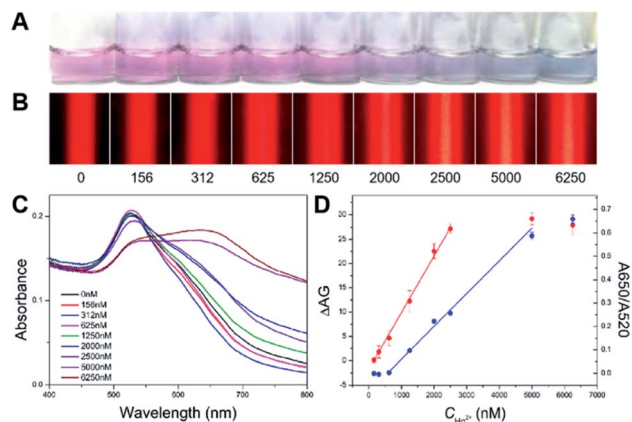
Fig. 5 (A) LSPR-related colorimetric results obtained from the detection of a series of Hg^{2+} samples in buffer with varying analyte concentrations (nM). (B) TE images recorded for the reaction solutions shown in (A). (C) UV-vis spectra measured from the mixtures provided in (A). (D) Calibration curves plotted by the tested Hg^{2+} concentration ($C_{Hg^{2+}}$) values *vs.* the ratios of the absorbance values recorded at 650 and 520 nm in the spectra shown in (C) (A650/A520; blue curve) and the ΔAG ($AG_{Hg^{2+}} - AG_{blank}$) values (red curve). Each error bar represents the standard deviation of three replicate experiments.

aggregation led to the gradual red-to-blue color change in the final reaction solutions. The LSPR-based naked-eye limit of detection (LOD) for the Hg^{2+} was qualitatively judged to be 1250 nM. At this analyte level, the resultant solution displayed a red color; but it was still different from that observed in the case of the blank sample (0 nM analyte). Moreover, the UV-vis spectra were recorded for all of these samples (Fig. 5C). Various spectrum profiles were produced because of different degrees of the Hg^{2+} level-dependent AuNP aggregation. It was found that the ratio of absorbance at 650 and 520 nm (A650/A520) was linear over the Hg^{2+} concentration ($C_{Hg^{2+}}$) in a range of 625–5000 nM (Fig. 5D, blue curve) with a regression equation of $y = 0.00014x - 0.07958$ ($R^2 = 0.988$). The UV-vis quantitative LOD was estimated to be ~87 nM based on the 3σ rule.

For the new method with the TE signaling, Fig. 5B shows that the TE intensity increases with the increase in the Hg^{2+} concentration from 0 to 5000 nM that enables the increased AuNP aggregation, which thus indicates a positive correlation between the visual response and the analyte level. However, when the analyte concentration continues to increase up to 6250 nM, a slightly decreased TE response was observed, presumably due to the sedimentation of oversized aggregates and the removal of partial thiolated oligonucleotides from the AuNPs' surfaces by excessive analyte ions (because of their thiophilic nature) leading to less particle aggregation. By comparing the background TE signal for the blank sample, the visual LOD of the TEA for the Hg^{2+} was determined to ~625 nM. Fig. 5D additionally shows the calibration curve that depicts the relationship between the calculated ΔAG ($AG_{Hg^{2+}} - AG_{blank}$) values and the tested Hg^{2+} levels (red curve). The ΔAG was linearly proportional to the $C_{Hg^{2+}}$ value range from 156 to 2500 nM. The corresponding regression equation was $y = 0.0116x - 1.7690$ ($R^2 = 0.998$), from which a quantitative LOD of ~25 nM was calculated for the analyte ion (3σ). It is noted that this LOD was achieved by the TEA method with only a laser pointer pen and a smartphone and is ~3 times lower than that obtained from the LSPR method using the UV-vis spectrometer. Furthermore, this developed new method was also compared with many recent LSPR-based colorimetric Hg^{2+} nanosensors with AuNPs and functional nucleic acids. As can be seen in Table 1, our instrument-free TEA is able to provide comparable or even better analytical performance in terms of LOD, cost, analysis time and portability.

Finally, to verify the practicality and reliability of the new method, it was further used to detect Hg^{2+} ions in several real water samples, *i.e.*, tap water, drinking water, and pond water. Before the analysis, potential interferences existing in these collected samples were removed as much as possible by filtering them with nanoporous membranes. The recovery results obtained were within the range from 93.68 to 108.71% (Table S1 in ESI†). The relative standard deviations (RSDs) calculated were

Table 1 Comparison of the new Hg^{2+} assay with some previous colorimetric ones using AuNPs probes and thymine-rich functional nucleic acids

Signaling method	Quantifying method	Portability	LCR[a] (µM)	LOD[b] (nM)	Time (min)	Ref.
LSPR	UV-vis	No	25–750	50	40	21
LSPR	UV-vis	No	0.5–5	250	10	31
LSPR	UV-vis	No	0–10	1000	5	32
LSPR	UV-vis	No	0.05–0.3	15	25	33
LSPR	UV-vis	No	0–5	500	32	39
LSPR	UV-vis	No	2–40	2000	35	40
LSPR	UV-vis	No	0.05–0.5	30	62	41
LSPR	UV-vis	No	0.2–6	50	10	42
LSPR	UV-vis	No	0.25–1.25	50	120	43
LSPR	UV-vis	No	0.75–1.5	250	22	44
LSPR	UV-vis	No	0.005–10	3.4	60	45
TE	Smartphone	Yes	0.156–2.5	25	10	This work

[a] LCR: linear concentration range. [b] LOD: limit of detection.

between 0.85 and 6.99% ($n = 3$). The acceptable results should be attributed to the use of the Hg^{2+}-specific functional ssDNAs, thus indicating the practicality of our method for the highly selective determination of the analyte ion in complex water samples.

Conclusions

We have successfully established a TE-based nanosensing method for highly sensitive, specific, colorimetric detection of Hg^{2+} at the nanomolar levels, based on the analyte-triggered "double" aggregation and TE enhancement of the bare AuNPs via unique T–Hg^{2+}–T coordination chemistry. The TEA approach just required the operator to use a quite inexpensive laser pointer pen to rapidly achieve naked-eye qualitative analysis of 625 nM Hg^{2+} within 10 min. A mobile smartphone could be additionally adopted as quantitative reader for accurately determining the analyte level with a limit downto 25 nM. Moreover, the satisfactory specificity and recovery results also demonstrated the practicability of our biosensor. The comparison study confirmed that it was superior to most of recent AuNP-based visual Hg^{2+} assays with the T-rich functional nucleic acids and LSPR signaling for its simplicity, high sensitivity, analytical efficiency, and portability. We believe the proposed equipment-free Hg^{2+} nanosensor with the TE as signal readout would hold great promise to be further optimized as a sustainable tool for particularly point-of-use applications like on-site environmental monitoring and household water safety assessment.

Conflicts of interest

There are no conflicts to declare.

Acknowledgements

References

1 G. Sener, L. Uzun and A. Denizli, *Anal. Chem.*, 2014, **86**, 514–520.
2 Z. Duan, X. Zhang, T. Ye, X. Zhang, S. Dong, J. Liu, X. Xiao and C. Jiang, *ACS Appl. Mater. Interfaces*, 2018, **10**, 25737–25743.
3 J. Du, M. Liu, X. Lou, T. Zhao, Z. Wang, Y. Xue, J. Zhao and Y. Xu, *Anal. Chem.*, 2012, **84**, 8060–8066.
4 N. Logan, C. McVey, C. Elliott and C. Cao, *Nano Res.*, 2020, **13**, 989–998.
5 S. L. C. Ferreira, M. A. Bezerra, A. S. Santos, W. N. L. dos Santos, C. G. Novaes, O. M. C. de Oliveira, M. L. Oliveira and R. L. Garcia, *TrAC, Trends Anal. Chem.*, 2018, **100**, 1–6.
6 O. Zverina, J. Kuta, P. Coufalik, P. Koseckova and J. Komarek, *Food Chem.*, 2019, **298**, 125084.
7 F. X. Han, W. D. Patterson, Y. Xia, B. B. M. Sridhar and Y. Su, *Water, Air, Soil Pollut.*, 2006, **170**, 161–171.
8 S.-Y. Huang, S.-J. Jiang and A. C. Sahayam, *Spectrochim. Acta, Part B*, 2014, **101**, 46–50.
9 R. Ranaweera, C. Ghafari and L. Luo, *Anal. Chem.*, 2019, **91**, 7744–7748.
10 H. Chen, J. Chen, X. Jin and D. Wei, *J. Hazard. Mater.*, 2009, **172**, 1282–1287.
11 Q. Zhou, M. Lei, Y. Liu, Y. Wu and Y. Yuan, *Talanta*, 2017, **175**, 194–199.
12 C. Chen, J. Zhao, Y. Lu, J. Sun and X. Yang, *Anal. Chem.*, 2018, **90**, 3505–3511.
13 W. M. He, Z. Zhou, Z. Han, S. Li, Z. Zhou, L. F. Ma and S. Q. Zang, *Angew. Chem., Int. Ed.*, 2021, **60**, 8505–8509.
14 A. Amirjani and D. H. Fatmehsari, *Talanta*, 2018, **176**, 242–246.
15 C. Chen, D. Zhao, B. Wang, P. Ni, Y. Jiang, C. Zhang, F. Yang, Y. Lu and J. Sun, *Anal. Chem.*, 2020, **92**, 4639–4646.
16 X. Liu, F. He, F. Zhang, Z. Zhang, Z. Huang and J. Liu, *Anal. Chem.*, 2020, **92**, 9370–9378.
17 J. Xiao, Y. Liu, L. Su, D. Zhao, L. Zhao and X. Zhang, *Anal. Chem.*, 2019, **91**, 14803–14807.
18 J. Dai, H. Zhang, C. Huang, Z. Chen and A. Han, *Anal. Chem.*, 2020, **92**, 16122–16129.
19 Y. Zhou, X. Huang, C. Liu, R. Zhang, X. Gu, G. Guan, C. Jiang, L. Zhang, S. Du, B. Liu, M. Y. Han and Z. Zhang, *Anal. Chem.*, 2016, **88**, 6105–6109.
20 H. Wang, L. Yang, S. Chu, B. Liu, Q. Zhang, L. Zou, S. Yu and C. Jiang, *Anal. Chem.*, 2019, **91**, 9292–9299.
21 G. H. Chen, W. Y. Chen, Y. C. Yen, C. W. Wang, H. T. Chang and C. F. Chen, *Anal. Chem.*, 2014, **86**, 6843–6849.
22 L. Yang, W. Yun, Y. Chen, H. Wu, X. Liu, M. Fu and Y. Huang, *Microchim. Acta*, 2017, **184**, 4741–4747.
23 Y. Ding, S. Wang, J. Li and L. Chen, *TrAC, Trends Anal. Chem.*, 2016, **82**, 175–190.
24 J. Yang, Y. Zhang, L. Zhang, H. Wang, J. Nie, Z. Qin, J. Li and W. Xiao, *Chem. Commun.*, 2017, **53**, 7477–7480.
25 W. Xiao, Z. Deng, J. Huang, Z. Huang, M. Zhuang, Y. Yuan, J. Nie and Y. Zhang, *Anal. Chem.*, 2019, **91**, 15114–15122.
26 Z. Deng, W. Jin, Q. Yin, J. Huang, Z. Huang, H. Fu, Y. Yuan, J. Zou, J. Nie and Y. Zhang, *Chem. Commun.*, 2021, **57**, 2613–2616.
27 J. Huang, X. Mo, H. Fu, Y. Sun, Q. Gao, X. Chen, J. Zou, Y. Yuan, J. Nie and Y. Zhang, *Sens. Actuators, B*, 2021, **344**, 130218.
28 P. Comtois, *Aerobiologia*, 2001, **17**, 193–202.
29 D. B. Rootman, J. L. Lin and R. Goldberg, *Ophthalmic Plast. Reconstr. Surg.*, 2014, **30**, 524–527.
30 B. Groever, B. Heshmat and R. Raskar, *ACS Photonics*, 2016, **3**, 930–935.
31 C. W. Liu, Y. T. Hsieh, C. C. Huang, Z. H. Lin and H. T. Chang, *Chem. Commun.*, 2008, 2242–2244.

32 X. J. Xue, F. Wang and X. G. Liu, *J. Am. Chem. Soc.*, 2008, **130**, 3244–3245.

33 A. G. Memon, X. Zhou, J. Liu, R. Wang, L. Liu, B. Yu, M. He and H. Shi, *J. Hazard. Mater.*, 2017, **321**, 417–423.

34 X. Zhang, M. R. Servos and J. Liu, *J. Am. Chem. Soc.*, 2012, **134**, 7266–7269.

35 Y. Deng, X. Wang, F. Xue, L. Zheng, J. Liu, F. Yan, F. Xia and W. Chen, *Anal. Chim. Acta*, 2015, **868**, 45–52.

36 Y. Hao, Y. Li, L. Song and Z. Deng, *J. Am. Chem. Soc.*, 2021, **143**, 3065–3069.

37 Q. Shen, Z. Nie, M. Guo, C. J. Zhong, B. Lin, W. Li and S. Yao, *Chem. Commun.*, 2009, **8**, 929–931.

38 J. W. Park and J. S. Shumaker-Parry, *J. Am. Chem. Soc.*, 2014, **136**, 1907–1921.

39 X. Xu, J. Wang, K. Jiao and X. Yang, *Biosens. Bioelectron.*, 2009, **24**, 3153–3158.

40 Y. Zhang, W. Liu, W. Zhang, S. Yu, X. Yue, W. Zhu, D. Zhang, Y. Wang and J. Wang, *Biosens. Bioelectron.*, 2015, **72**, 218–224.

41 Q. Wang, X. Yang, X. Yang, P. Liu, K. Wang, J. Huang, J. Liu, C. Song and J. Wang, *Spectrochim. Acta, Part B*, 2015, **136**, 283–287.

42 Y. Xu, L. Deng, H. Wang, X. Ouyang, J. Zheng, J. Li and R. Yang, *Chem. Commun.*, 2011, **47**, 6039–6041.

43 T. Li, S. Dong and E. Wang, *Anal. Chem.*, 2009, **81**, 2144–2149.

44 Z. Qing, X. He, K. Wang, Z. Zou, X. Yang, J. Huang and G. Yan, *Anal. Methods*, 2012, **4**, 3320–3325.

45 S. Liu, X. Leng, X. Wang, Q. Pei, X. Cui, Y. Wang and J. Huang, *Microchim. Acta*, 2017, **184**, 1969–1976.